Publications

Available Online

J. Sci. Res. **17** (2), 427-439 (2025)

JOURNAL OF SCIENTIFIC RESEARCH

www.banglajol.info/index.php/JSR

Surface Roughness Effect on Porous Pivoted Slider Bearings with Squeeze Film Formed by Couple Stress Fluid

B. Kashinath[1], A. C. Upadhya[2*]

[1]Department of Mathematics, Government First Grade College, Sedam, Karnataka, India

[2]Department of Mathematics, Sangolli Rayanna First Grade Constituent College, Belagavi, Karnataka, India

Received 21 August 2024, accepted in final revised form 3 December 2024

Abstract

The study intends to investigate the problem of surface roughness effects on porous pivoted slider bearings with squeeze film formed by couple stress fluid. On the basis of the micro continuum theory, the modified Reynolds' type equation of porous slider bearing is obtained by considering rough surface and squeezing action. The closed-form expressions for the mean pressure, load carrying capacity, frictional force and centre of pressure are obtained. Capacity for load bearing and point where pressure is centred are evaluated in form of various parameters that are couple stress, permeability and surface roughness. It is concluded that capacity for load bearing increases with roughness and decreases with increase in permeability parameters. Normal behaviour of exists for surface roughness parameters with pressure and pressure with permeability parameters. Computed values of load capacity, frictional force and coefficient of friction are displayed in graphical form.

Keywords: Porous; Squeeze film; Couple stress; Slider bearing.

doi: https://dx.doi.org/10.3329/jsr.v17i2.75553 J. Sci. Res. **17** (2), 427-439 (2025)

1. Introduction

Hydrodynamic bearings are commonly used in various machines. The slider bearing being the most common and simplest type among them. Probably, this is because the expression for film thickness is simple and the boundary conditions required to be zero at the bearing ends are less complicated. Because the film in slider bearings is continuous and non-diverging the issue of negative pressure is avoided. These bearings are designed to support the axial loads. Slider bearings are often designed for supporting the transverse load in engineering applications. Bearing characteristics for different film shapes have been analyzed by Pinkus and Sternlicht [1], Bagci and Singh [2], Hamrock [3] etc.

Squeeze films play an important role in engineering practice. The application of squeeze film slider bearings in clutch plates, automobile transmissions and domestic appliances

*Corresponding author: adinatha06@gmail.com

many investigators dealt with the problem of squeeze film slider bearing such as Prakash and Vij [4], Bhat [5], Bhat and Patel [6] etc.

The fluid flow through porous media has been an interesting area of research for the last five decades. Many industrial, geologists, hydrologists and several other researchers have been attracted to study the flow behavior in a porous medium. In a macroscopic scale the fluid flow in an isotropic and homogeneous porous medium is governed by Darcy's law [7] or Brinkman's equations [8]. There have been numerous analytical studies of porous bearings including the work by Cameron *et al.* [9], Murati [10], Wu [11], Uma [12] and Naduvinamani *et al*. [13]. They all found that when permeability increases the drag force decreases because high permeability offers less resistance to flow through the porous interior.

In recent years surface roughness and its effects on machine design have been intensively investigated to determine how they affect flow patterns. Some mathematical models have been proposed to derive the different Reynold's types by considering the surface roughness effects. Averaging fluid film thicknesses or flow quantities between two lubricated roughness has been used to analyze surface effects. The effect of surface roughness, Christensen [14,15] utilized a stochastic concept and introduced an averaging film model to lubricated surfaces with straightened roughness. The stochastic Reynold's type equations of rough bearing were derived and applied to investigate the effects of surface roughness on the bearing performance characteristics. Several investigators have adopted a stochastic approach to model the random roughness. Christensen and Tonder [16] presented a comprehensive general analysis of surface roughness (both transverse and longitudinal) based on a general probability density function by modifying and developing the approach of Tzeng and Seibel [17]. Subsequently, on the ground of this Christensen and Tonder's stochastic model, many researchers have been carried out the study of the effect of surface roughness on hydrodynamic mechanisms, such as the works in the hydrodynamics journal bearing by Guha [18] and Taranga *et al.* [19]. The squeeze film spherical bearings by Andharia *et al.* [20]. Lin *et al.* [21] and Naduvinmani *et al.* [22] used this theory for the study of surface roughness effects on different bearing systems.

The motion of non-Newtonian fluids has numerous important uses in modern technology and industries. This has prompted several researchers to explore various flow issues associated with several types of non-Newtonian fluids. A couple stress fluid proposed by Stoke's [23] during the last five decades has attracted the attention of numerous researchers in fluid mechanics. A couple stress fluid theories are a simple generalization of a Newtonian fluid theory that allows the sustenance of couple stresses and body couples. A couple stresses arise as a result of the mechanical interactions in the fluid medium being modelled. This stress tensor is not symmetric, it adequately describes the flow behavior of fluids with a substructure such as lubricating oils, liquid crystals and animal blood. In numerous studies of hydrodynamic lubrication of squeeze film flows, the lubricant has been considered as a couple stress fluid and these studies have shown that couple stress fluids increase the bearing's load capacity. Ramanaiah [24] analyzed squeeze films between finite plates lubricated by fluids with couple stress. Naduvinamani *et al*. [25] have analyzed

hydrodynamic lubrication of rough slider bearings with couple stress fluids. Rao and Agarwal [26] studied the problem of the effects of couple stresses on the performance of rough step slider bearings with assorted porous structures. Naduvinamani *et al*. [27] studied the static and dynamic characteristics of porous plane inclined slider bearings lubricated with magnetohydrodynamic couple stress fluid. Surface roughness effects on curved pivoted slider bearings with coupe stress fluid were discussed by Naduvinmani and Biradar Kashinath [28]. Nisha *et al.* [29] studied the squeeze film characteristics and steady-state performance of a parabolic inclined porous slider bearing using couple stress fluid. Panchal, *et al.* [30] studied, Effect of Various Shapes of Rough Transverse Slider Bearing Equipped with Ferro-Lubricant on the Load-Tolerating Capability by Mathematical Modeling.

In this paper the effect of surface roughness on porous pivoted slider bearings lubricated with couple stress fluid was studied, along with squeeze film action, on which a study has not been conducted so far as per the relevant literature. An averaged modified Reynold's-type equation for rough porous pivoted slider bearings has been computed and numerical computations were carried out to get the required results.

2. Mathematical Formulation and Solution of the Problem

The basic equations governing the motion of an incompressible flow in deprivation of body forces and couples are given by,

$$\rho \frac{D\vec{V}}{Dt} = -\nabla p + \mu \nabla^2 \vec{V} - \eta \nabla^4 \vec{V}, \tag{1}$$

$$\nabla \cdot \vec{V} = 0 \tag{2}$$

where, ρ, p, μ and η represents density, pressure, coefficient of viscosity and material constant respectively.

The physical configuration of the curved pivoted porous slider bearings lubricated with couple stress fluid is shown in Fig. 1. It consists of two surfaces separated by a lubricant film. It is assumed that the upper surface is rough and is moving at a constant velocity U. While the lower porous matrix supported by a solid backing is at rest. It is assumed that the lubricant in the film region as well as in the porous region is assumed to be Stokes (1966) couple stress fluid. A stator with a central thickness of Hc (u,v), where u and v represent the fluid film's x and y velocity components. The thickness of film H, here h_0 and h_1 are minimum and maximum film thickness respectively. Also, the stator moves normally towards the lower surface-slider with the uniform velocity.

$$\dot{h} = \frac{dh}{dt} \tag{3}$$

where, *t* is time in seconds, is called squeeze velocity.

To represent the surface roughness the mathematical expression for the film thickness is considered to be consisting of two parts.

$$H(x) = h(x) + h_s \tag{4}$$

where,

$$h(x) = H_c \left\{ 4\left(\frac{x}{L} - \frac{1}{2}\right)^2 - 1 \right\} + h_0 \left(a - a\frac{x}{L} + \frac{x}{L} \right) \tag{5}$$

in which

$$a = \frac{h_1}{h_0}$$

where *h(x)* is the mean film thickness and h_s is a randomly varying quantity measured from the mean level and thus characterizes the surface roughness. Furthermore, h_s is considered to have probability density function $f(h_s)$ defined over the domain $-c \leq h_s \leq c$,where c is the maximum deviation from the mean film thickness. The mean $\alpha *$, the standard deviation $\sigma *$ and the pressure parameter $\varepsilon *$ which is the measure of the symmetry of the random variable h_s, are defined as

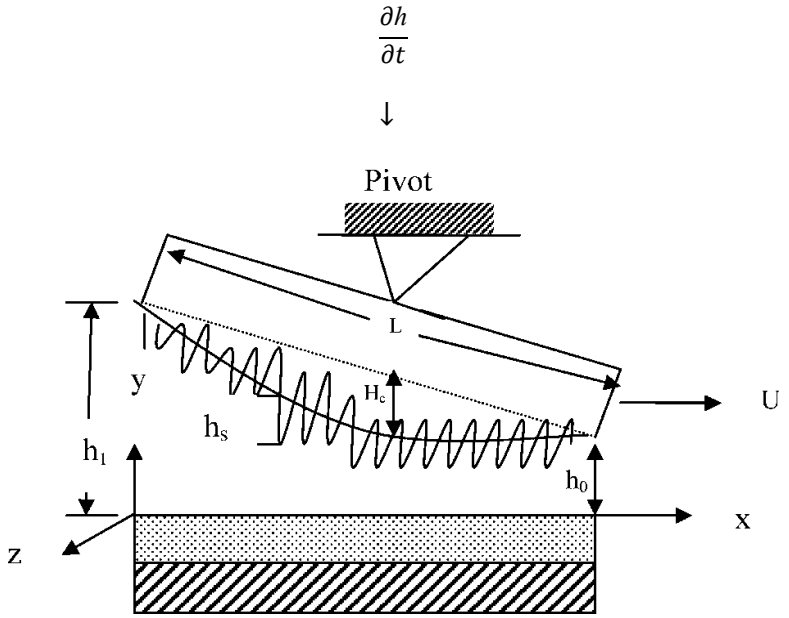

Fig. 1. Couple stress fluid lubricated curved pivoted porous slider bearings with squeeze velocity $\dot{h}$.

$$\alpha *= E(h_s) \tag{6}$$
$$\sigma *^2 = E[(h_s - \alpha)^2] \tag{7}$$
$$\varepsilon *= E[(h_s - \alpha)^3] \tag{8}$$

where E is an expectation operator defined by,

$$E(\cdot) = \int_{-\infty}^{\infty} (\cdot) f(h_s)\, dh_s \tag{9}$$

where the parameters $\alpha *$, $\sigma *$ and $\varepsilon *$ are all independent of *x*. The mean $\alpha *$and the parameter $\varepsilon *$ can assume both positive and negative values but $\sigma *$ can only assume positive values.

The porous region is assumed to be homogeneous and isotropic and the lubricant is incompressible couple stress fluid. It is assumed that body force and body couples are absent with the usual assumptions of hydrodynamic lubrication applicable to thin films. The equations of motions (1) and (2) take the following form in terms of Cartesian coordinates:

$$\frac{\partial u}{\partial x} + \frac{\partial v}{\partial y} = 0 \tag{10}$$

$$\boldsymbol{\mu}\frac{\boldsymbol{\partial^2 u}}{\boldsymbol{\partial y^2}} - \boldsymbol{\eta}\frac{\boldsymbol{\partial^4 u}}{\boldsymbol{\partial y^4}} = \frac{\boldsymbol{\partial p}}{\boldsymbol{\partial x}} \tag{11}$$

$$\frac{\partial p}{\partial y} = 0 \tag{12}$$

The flow of couple stress fluid in a porous matrix is governed by the modified form of Darcy's law for isotropic porous materials,

$$\vec{q}* = \frac{-k}{\mu(1-\beta)}\nabla p^* \tag{13}$$

where, $\vec{q}* = (u*, v*), \beta = \frac{\eta}{\mu\kappa}$ and the parameter κ is the permeability of the porous material and is known as pore size and β is the ratio of microstructure size to the pore size. If $\left(\frac{\eta}{\mu}\right)^{1/2} \approx \sqrt{k}$ i.e., $\beta \approx 1$ then the microstructure additives present in the lubricant block the pores in the porous layer and thus reduce the Darcy flow through the porous matrix. When the microstructure size is very small when compared with the porous size, $\beta << 1$ the additives percolate into the porous matrix. The limit $\beta \to 0^+$ equation (13) reduces to the usual Darcy's law. The pressure in the porous region due to continuity satisfies Laplace's equation:

$$\frac{\partial^2 p^*}{\partial x^2} + \frac{\partial^2 p^*}{\partial y^2} = 0 \tag{14}$$

The relevant boundary conditions for the velocity components are:

(i) At the upper solid surface (y = H)

$$u = \text{U}\ ,\ \frac{\partial^2 u}{\partial y^2} = 0 \tag{15a}$$

$$v = \frac{dh}{dt} \tag{15b}$$

(ii) At the lower surface (y = 0)

$$\boldsymbol{u = 0,\ \frac{\partial^2 u}{\partial y^2} = 0} \tag{16a}$$

$$v = v* \tag{16b}$$

Solving equation (11) with boundary conditions (15a) and (16a) the velocity components u can be derived as follows

$$u = \frac{Uy}{H} + \frac{1}{2\mu}\cdot\frac{\partial p}{\partial x}\left\{2l^2\left[1 - cosh\left(\frac{y}{l}\right) + sinh\left(\frac{y}{l}\right)tanh\left(\frac{y}{2l}\right)\right] + y^2 - yH\right\} \tag{17}$$

where $l = \left(\frac{\eta}{\mu}\right)^{1/2}$ is couple stress parameter.

Integrating equation (14) with respect to z over the porous layer thickness H and applying the boundary conditions $\frac{\partial p^*}{\partial y} = 0$ at y = - H, it is obtained,

$$\left(\frac{\partial p^*}{\partial y}\right)_{y=0} = -\int_{y=0}^{-H}\frac{\partial^2 p^*}{\partial x^2}\text{dy} \tag{18}$$

The porous layer thickness H is assumed to be very small and applying the pressure $p = p^*$ continuity condition of the interface $y = 0$ of porous matrix and fluid film, equation (18) reduces to:

$$\left(\frac{\partial p^*}{\partial y}\right)_{y=0} = -H\frac{\partial^2 p^*}{\partial x^2} \tag{19}$$

Substituting the expressions for u in the continuity equation (10) and integrating across the fluid film thickness and using the boundary conditions (16b) and (17b) for v gives the nonlinear modified Reynold's equation is:

$$\frac{\partial}{\partial x}\int_0^h u\,dy + v_{y=h} - v_{y=0} = 0 \tag{20}$$

yields,

$$\frac{\partial}{\partial x}\left\{12l^3\left(\begin{matrix}sinh\left(\frac{H}{l}\right) - cosh\left(\frac{H}{l}\right)tanh\left(\frac{H}{2l}\right) + tanh\left(\frac{H}{2l}\right) + \\ H^3 - 12l^2H - 12kH*\end{matrix}\right)\frac{\partial p}{\partial x}\right\} = 6\mu U\frac{dH}{dx} + 12\mu V \tag{21}$$

where $v_{y=h} = V = \frac{dh}{dt} = h$

The surface roughness parameters are used to get the following equation:

$$\frac{\partial}{\partial x}\left\{\left(\begin{matrix}h^3 + 3h^2\alpha* + 3h(\alpha*^2 + \sigma*^2 - 4l^2) + tanh\left(\frac{h}{2l}\right)(24l^3 - 6l\alpha*^2 - 6l\sigma*^2) + \\ tanh^2\left(\frac{h}{2l}\right)(4\varepsilon* + 4\alpha*^3 + 12\alpha*\sigma*^2 - 12l^2\alpha*) - 12kH*\end{matrix}\right)\frac{\partial \bar{p}}{\partial x}\right\}$$
$$= 6\mu U\frac{dh}{dx} + 12\mu V \tag{22}$$

where, $\alpha*, \sigma*$ and $\varepsilon*$ are the parameters due to surface roughness and $E(H) = h$ and $\mathrm{E}(p) = \bar{p}$

Using the following dimensionless quantities we get,

$$x^* = \frac{x}{L}, l^* = \frac{l}{h_0}, \beta = \frac{H_c}{H_0}, h^* = \frac{h}{h_0},\ p = \frac{p*{h_0}^2}{\mu UL},\ S = \frac{-2V\dot{L}}{Uh_0}, \psi = \frac{12kH*}{{h_0}^3}, \alpha = \frac{\alpha*}{h_0},$$
$$\sigma = \frac{\sigma*}{h_0}, \varepsilon = \frac{\varepsilon*}{{h_0}^3}$$

Equation (12) takes the form:

$$\frac{\partial}{\partial x*}\left\{\left(\begin{matrix}h^{*3} + 3h^{*2}\alpha + 3h*(\alpha^2 + \sigma^2 - 4l*^2) + tanh\left(\frac{h*}{2l}\right)(24l*^3 - 6l*\alpha^2 - 6l*\sigma^2) + \\ tanh^2\left(\frac{h*}{2l*}\right)(4\varepsilon + 4\alpha^3 + 12\alpha\sigma^2 - 12l*^2\alpha) - \psi\end{matrix}\right)\frac{\partial p*}{\partial x*}\right\} = \frac{dG}{dx*} \tag{23}$$

where,

$\mathrm{G} = 6h - 6Sx*$,

Equation (23) is known as the dimensionless Reynold's equation. Since the pressure is negligible on the boundaries of the slider bearing compared to inside pressure.

The pressure field boundary conditions are:

$p = 0$ at $x^* = 0{,}1$ (Ambient pressure) (24)

Integrating the equation of (23) with respect to x*

$$\frac{\partial p*}{\partial x*} = (G - Q)\left(\begin{matrix}h^{*3} + 3h^{*2}\alpha + 3h*(\alpha^2 + \sigma^2 - 4l*^2) + tanh\left(\frac{h*}{2l}\right)(24l*^3 - 6l*\alpha^2 - 6l*\sigma^2) + \\ tanh^2\left(\frac{h*}{2l*}\right)(4\varepsilon + 4\alpha^3 + 12\alpha\sigma^2 - 12l*^2\alpha) - \psi\end{matrix}\right)^{-1} \tag{25}$$

where Q is the constant of integration.

Solving equation (25) subject to the boundary conditions (24) which gives the dimensionless film pressure p* is obtained as:

$$p* = \int_{x*=0}^{x*}(G_1 - Q)\left(\begin{matrix}h^* + 3h^{*2}\alpha + 3h*(\alpha^2 + \sigma^2 - 4l*^2) + tanh\left(\frac{h*}{2l}\right)(24l*^3 - 6l*\alpha^2 \\ - 6l*\sigma^2) + tanh^2\left(\frac{h*}{2l*}\right)(4\varepsilon + 4\alpha^3 + 12\alpha\sigma^2 - 12l*^2\alpha) - \psi\end{matrix}\right)^{-1} dx* \tag{26}$$

where,

$$Q = \frac{\int_{x*=0}^{1}(G_1)\cdot\left(\begin{matrix}h^* + 3h^{*2}\alpha + 3h*(\alpha^2 + \sigma^2 - 4l*^2) + tanh\left(\frac{h*}{2l}\right)(24l*^3 - 6l*\alpha^2 - 6l*\sigma^2) + \\ tanh^2\left(\frac{h*}{2l*}\right)(4\varepsilon + 4\alpha^3 + 12\alpha\,\sigma^2 - 12l*^2\,\alpha) - \psi\end{matrix}\right)^{-1} dx*}{\int_{x*=0}^{1}\frac{1}{\left(\begin{matrix}h^*+3h^{*2}\alpha+3h*(\alpha^2+\sigma^2-4l*^2)+tanh\left(\frac{h*}{2l}\right)(24l*^3-6l*\alpha^2-6l*\sigma^2)+ \\ tanh^2\left(\frac{h*}{2l*}\right)(4\varepsilon+4\alpha^3+12\alpha\,\sigma^2-12l*^2\alpha)-\psi\end{matrix}\right)}dx*}$$

The load carrying capacity W^* are given in dimensionless form by,

$$W* = \frac{Wh_0{}^2}{\mu UL^2} = \int_0^1 p\ dx* \tag{27}$$

The component of the stress tensor required to calculate the frictional force is

$$\tau_{yx} = \mu\left(\frac{\partial u}{\partial y}\right) - \eta\left(\frac{\partial^3 u}{\partial y^3}\right) \tag{28}$$

The frictional force F^* per unit width on the sliding bearing pivoted surface is given by,

$$F = \int_0^L (\tau_{yx})_{y=H}\, dx \tag{29}$$

Use of expression (8) for u in equation (16) and substituting it in equation (17) gives frictional force which after dimensionless becomes,

$$F* = \int_0^1 \left[\frac{h*}{2}\cdot\left((G-Q)\left(\begin{matrix}h^{*3} + 3h^{*2}\alpha + 3h*(\alpha^2 + \sigma^2 - 4l*^2) + \\ tanh\left(\frac{h*}{2l}\right)(24l*^3 - 6l*\alpha^2 + -6l*\sigma^2) \\ tanh^2\left(\frac{h*}{2l*}\right)(4\varepsilon + 4\alpha^3 + 12\alpha\,\sigma^2 - 12l*^2\,\alpha) - \psi\end{matrix}\right)^{-1}\right) + \frac{1}{h*}\right] dx* \tag{30}$$

The coefficient of friction is:

$$f* = \frac{F*}{W*} \tag{31}$$

The location of the centre of pressure where the resultant force acts are,

$$x* = \frac{X}{L} = \frac{1}{W*}\int_0^1 p*\cdot\ x*\ dx* \tag{32}$$

3. Results and Discussion

In the present paper the effects of bearing surface roughness, the permeability of the porous bearing and the couple stresses present in the lubricant due to micro structure additives are examined with the help of the dimensionless roughness parameters σ (standard deviation), α (mean), ε (symmetry of surface roughness), the permeability parameter ψ, the couple stress parameter l^* and the squeeze velocity.

3.1. *Fluid film pressure*

The graphs illustrated in Figs. 2 to 6 represent variation in non-dimensional pressure p^* against x^* with the effect of squeeze velocity $\dot{h}\neq 0$. In Fig. 2 by fixing the values a=3.0, S=0.5, σ=0.1, α =0.05, ε =0.05, β=0.3, ψ=0.001 for different values of l^*, it is found that the non-dimensional pressure p^* increases for the couple stress fluids as compared to the corresponding Newtonian case (l^*=0). The variation of p^* with x^* for different values of α, ε and σ is depicted in Figs. 3 to 5 respectively. It can be seen that p^* increases for the negatively skewed surface roughness and decreases for the positively skewed surface roughness pattern. Furthermore, p^* decreases for increasing σ values. Fig. 6 by fixing a=3.0, S=0.5, σ=0.1, α=0.05, ε=0.05, β=0.3, ψ=0.01 for different values of ψ, it is observed that

p^* decreases for increasing values of ψ. It is also interesting to note that the point of maximum pressure x^*_{max} shifts towards the inlet edge for increasing values of ψ.

3.2. *Load carrying capacity*

The graphs illustrated in Figs. 7 to 11 represent variation in non-dimensional load W* against the curvature parameter β with the effect of squeeze velocity $\dot{h}\neq 0$. In Fig. 7 by fixing the values a=3.0, S=0.5, σ=0.1, α =0.05, ε =0.05, ψ=0.001 for different values of l^*, it is noted that the bearings with couple stress fluid as lubricant carry a larger load as compared to the corresponding Newtonian case (l^*=0). Figs. 8 and 9 respectively show the effect of α and ε on the variations of W* with β. It is found that negatively skewed surface roughness increases W* whereas positively skewed surface roughness decreases W*. In Fig. 10 by fixing a=3.0, S=0.5, α=0.05, ε=0.05, l^*=0.3, ψ=0.001 and increasing values of σ the load carrying capacity W* decreases. In Fig. 11 by fixing a=3.0, S=0.5, σ=0.1, α=0.05, ε=0.05, l^*=0.3 and increasing values of ψ the load–carrying capacity W* found to be decreasing. Fig. 12 shows the variation in non-dimensional load W* against the curvature parameter β for different values of $\dot{h}$ with $l^*=0.5$, s*=0.3, ψ =0.001, h_0 =0.02, L=0.005 and U= 1.0 and it is found that W^* increases considerably in the presence of squeeze velocity.

3.3. *Coefficient of friction*

The graphs illustrated in Figs. 13 to 17 represent variation in the non-dimensional coefficient of friction f^* against the curvature parameter β with the effect of squeeze velocity $\dot{h}\neq 0$. In Fig. 13 by fixing the values a=3.0, S=0.5, σ=0.1, α =0.05, ε =0.05, ψ=0.001 for different values of l^* a drastic decrease in the coefficient of friction f^* is observed for the couple stress lubricants as compared to the corresponding Newtonian case (l^*=0). Figs. 14 and 15 respectively show the effect of α and ε on the variations of f^* with β, it is found that negatively skewed surface roughness decreases f^* whereas positively skewed surface roughness increases f^*. In Fig. 16 by fixing a=3.0, S=0.5, α=0.05, ε=0.05, l^*=0.3, ψ=0.001 and increasing values of σ the load carrying capacity W* increases. The coefficient of friction f^* decreases for increasingly negative values of α and ε whereas the coefficient of friction f^* increases for the increasingly positive values of α and ε. Also, f^* increases for increasing σ values. In Fig. 17 by fixing a=3.0, S=0.5, σ=0.1, α=0.05, ε=0.05, β=0.3, l^*=0.3 and increasing values of ψ the coefficient of friction f^* found to be increasing.

3.4 *Centre of pressure*

The graphs illustrated in Figs. 18 to 22 represent variation in the non-dimensional center of pressure x* against the curvature parameter β with the effect of squeeze velocity $\dot{h}\neq 0$. It can be seen that the center of pressure shifts towards the outlet edge for negatively skewed surface roughness, whereas it shifts towards the inlet edge for positively skewed surface roughness.

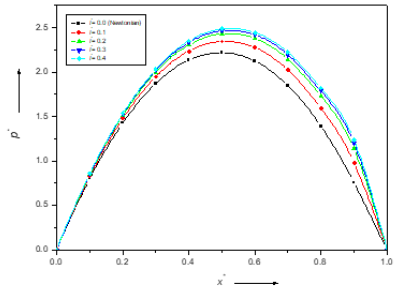

Fig. 2. Variation of non-dimensional pressure p^* with x^* for different values of couple stress l^*, with a=3.0, S=0.5, σ=0.1, α=0.05, ε=0.05, β =0.3, ψ=0.001.

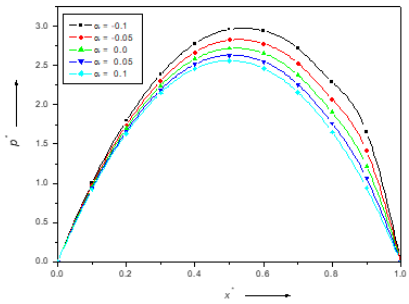

Fig. 3. Variation of non-dimensional pressure p^* with x^* for different values of α with a=3.0, S=0.5, l^*=0.3, σ=0.1, ε=0.05, β =0.3, ψ=0.001.

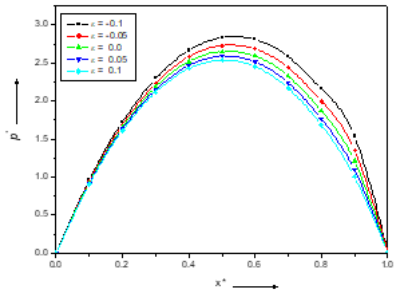

Fig. 4. Variation of non-dimensional pressure p^* with x* for different values of ε with a=3.0, S=0.5, l^*=0.3, σ=0.1, α =0.05, β =0.3, ψ=0.001.

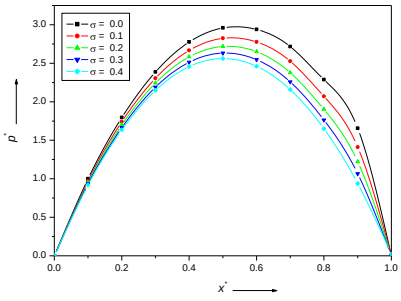

Fig. 5. Variation of non-dimensional pressure p^* with x^* for different values of σ with a=3.0, S=0.5, l^*=0.3, ε=0.05, α=0.05, β =0.3, ψ=0.001.

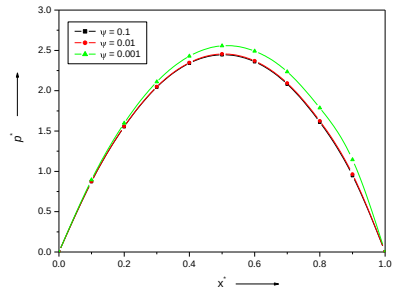

Fig. 6. Variation of non-dimensional pressure p^* with x^* for different values of ψ with a=3.0, S=0.5, l^*=0.3, ε =0.05, α =0.05, β =0.3, σ =0.1

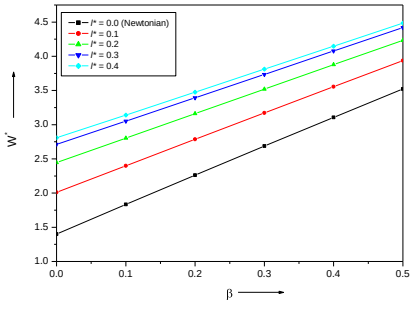

Fig. 7. Variation of non-dimensional load W* with β for different values of couple stress l^* with a=3.0, S=0.5, σ=0.1, α=0.05, ε=0.05, ψ=0.001.

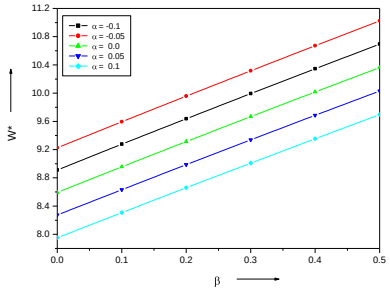

Fig. 8. Variation of non-dimensional load W* with β for different values of αwith a=3.0, S=0.5, σ=0.1, l*=0.03, ε=0.05, ψ=0.001.

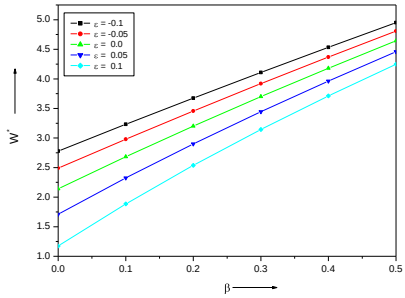

Fig. 9. Variation of non-dimensional load W* with β for different values of ε, with a=3.0, S=0.5, σ=0.1, l*=0.03, α =0.05, ψ=0.001.

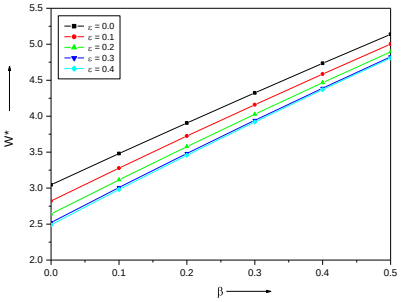

Fig. 10. Variation of non-dimensional load W* with β for different values of σ, with a=3.0, S=0.5, ε =0.05, l*=0.03, α =0.05, ψ=0.001.

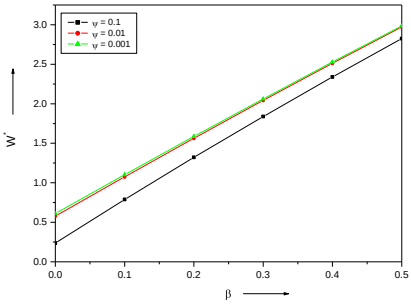

Fig. 11. Variation of non-dimensional load W* with β for different values of with ψ, a=3.0, S=0.5, ε =0.05, l*=0.03, α =0.05, σ=0.1.

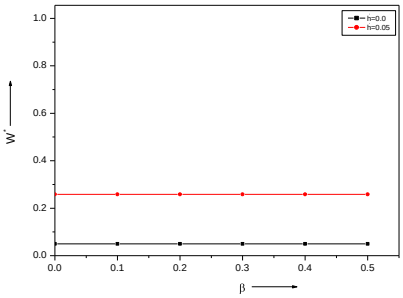

Fig. 12. Variation of the non-dimensional load W* with a* for different values of $\dot{h}$ with s*=0.3, S=0.5, l* =0.3, β =0.3, ψ=0.001, h_0 =0.02, L=0.005 and U=1.0.

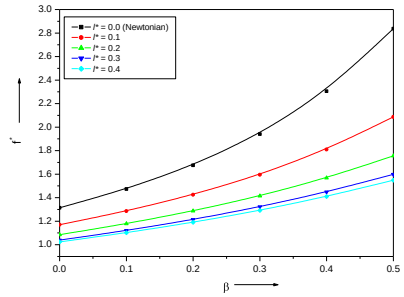

Fig. 13. Variation of non-dimensional coefficient of friction f* with β for different values of couple stress l*, with, a=3.0, S=0.5, ε = 0.05, α =0.05, σ=0.1, ψ=0.001.

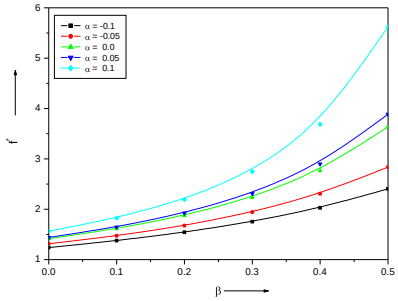

Fig. 14. Variation of non-dimensional coefficient of friction f* with β for different values of α, with, a=3.0, S=0.5, $l^*=0.3$, ε =0.05, σ=0.1, ψ=0.001.

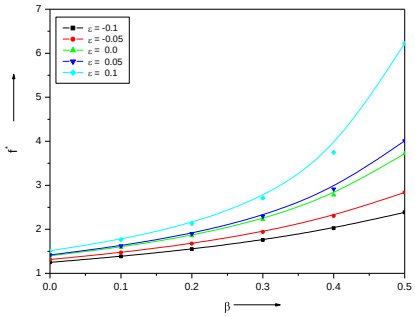

Fig. 15. Variation of non-dimensional coefficient of friction f* with β for different values of ε, with, a=3.0, S=0.5, $l^*=0.3$, α =0.05, σ=0.1, ψ=0.001.

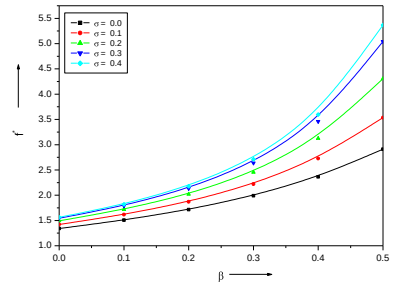

Fig. 16. Variation of non-dimensional coefficient of friction f* with β for different values of σ, with, a=3.0, S=0.5, $l^*=0.3$, α =0.05, ε =0.05, ψ=0.001.

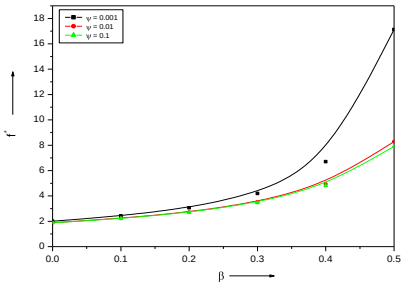

Fig. 17. Variation of non-dimensional coefficient of friction f* with β for different values of ψ, with, a=3.0, S=0.5, l^*=0.3, α =0.05, ε =0.05, σ=0.1.

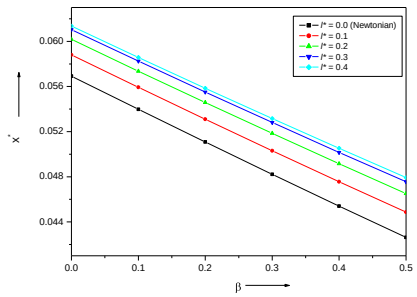

Fig. 18. Variation of non-dimensional center of pressure x*with β for different values of couple stress l^*, with, a=3.0, S=0.5, ε =0.05, α =0.05, σ=0.1,ψ=0.001.

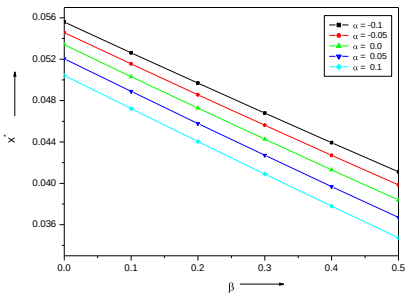

Fig. 19. Variation of non-dimensional center of pressure x*with β for different values of α, with, a=3.0, S=0.5, $l^*=0.3$, ε =0.05, σ=0.1, ψ=0.001.

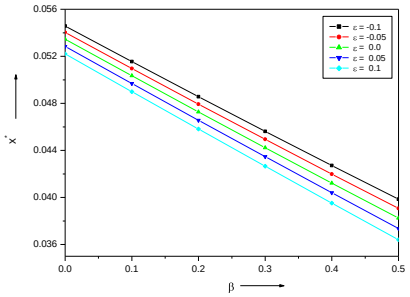

Fig. 20. Variation of non-dimensional center of pressure x* with β for different values of ε, with, a=3.0, S=0.5, $l^*=0.3$, α =0.05, σ=0.1, ψ=0.001.

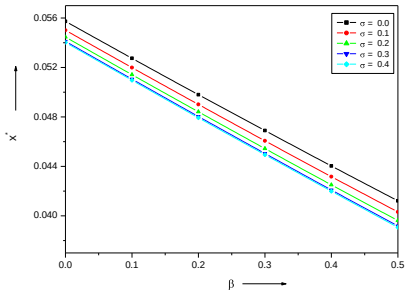

Fig. 21. Variation of non-dimensional center of pressure x* with β for different values of σ, with, a=3.0, S=0.5, $l^*=0.3$, α =0.05, ε =0.05, ψ=0.001.

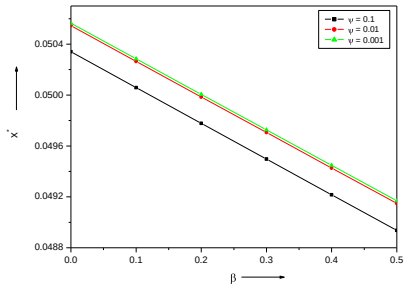

Fig. 22. Variation of non-dimensional center of pressure x* with β for different values of ψ, with, a=3.0, S=0.5, $l^*=0.3$, α =0.05, ε =0.05, σ =0.1.

4. Conclusions

In this chapter, the performance of rough porous pivoted slider bearings based on Darcy's law and Stoke's micro-continuum theory was studied. Based on the numerical computation of the results for various values of the dimensionless parameters the following important conclusions are drawn:

The use of couple stresses in the lubricant due to microstructure additives provides an increased load-carrying capacity and decreased coefficient of friction. The steady load carrying capacity decreases with increases in the value of permeability. The center of pressure shows normal behavior with permeability parameters. The presence of negatively (positively) skewed surface roughness provides an increase (decrease) in load-carrying capacity. The load-carrying capacity of bearings increases with increasing values of the curvature parameter but at the same time coefficient of friction also increases.

References

1. O Pinkus and B Strenlicht, Theory of Hydrodynamic Lubrication (McGraw-Hill, NY, USA, 1961). https://doi.org/10.1115/1.3636485
2. C. Bagci and A. P. Singh, ASLE Trans. J. Lub. Tech. **105**, 48 (1983). https://doi.org/10.1115/1.3254546
3. B. J. Harmrock, Fundamentals of Fluid Film Lubrication (McGraw-Hill, NY, USA, 1994). https://doi.org/10.1201/9780203021187.
4. J. Prakash and S. K. Vij, J. Mech. Eng. Sci. **15**, 232 (1973). https://doi.org/10.1243/JMES_JOUR_1973_015_039_02
5. M. V. Bhat, Jap. J. App. Phys.**17**, 479 (1978). https://doi.org/10.1143/JJAP.17.479
6. M. V. Bhat and C. M. Patel, Wear **66**, 189 (1981). https://doi.org/10.1016/0043-1648(81)90113-7
7. J. Bear, Courier Corporation **20**, 162 (1975).
8. H. C. Brinkman, Turbul. Combust. **1**, 27 (1949). https://doi.org/10.1007/BF02120313
9. A. Cameron, V. T. Morgan, and A. E. Satainshy, Proc. Inst. Mech. Eng. London **176**, 761 (1962). https://doi.org/10.1243/PIME_PROC_1962_176_061_02
10. S. Uma, Wear **42**, 205 (1977). https://doi.org/10.1016/0043-1648(77)90052-7
11. P. R. K. Maruti, Wear **18**, 449 (1971). https://doi.org/10.1016/0043-1648(71)90169-4
12. H. Wu, J. Lubri. Technol. **94**, 64 (1972). https://doi.org/10.1115/1.3451637
13. N. B. Naduvinamani and A. Siddangouda, J. Eng. Tribol. **221**, 615 (2007). https://doi.org/10.1243/13506501JET206
14. H. Christensen, Wear **17**, 149 (1971). https://doi.org/10.1016/0043-1648(71)90025-1
15. H. Christensen, Proc. Inst. Mech. Eng. **184**, 1013 (1969-70). https://doi.org/10.1243/PIME_PROC_1969_184_074_02
16. H. Christensen and K. Tonder, J. Lubricat. **93**, 324 (1971). https://doi.org/10.1115/1.3451579
17. S. T. Tzeng, and E. Saibel, Trans. ASLE **10**, 334 (1967). https://doi.org/10.1080/05698196708972191
18. S. K. Guha, Wear **167**, 173 (1993). https://doi.org/10.1016/0043-1648(93)90322-D
19. R. Turanga, A. S. Sekhar, and B. C. Majumdar, Tribol. Int. **32**, 231 (1999). https://doi.org/10.1016/S0301-679X(99)00035-3
20. P. I. Andharia, G. M. Deheri, and J. L. Gupta, Int. J. Appl. Mech. Eng. **6**, 885 (2001). https://doi.org/10.1080/10402009608983508
21. J. R. Lin, Comput. Struct. **80**, 297 (2002). https://doi.org/10.1016/S0045-7949(02)00003-2
22. N. B. Naduvinamani, S. T. Fathima, and P. S. Hiremath, Tribol. Int. **36**, 949 (2003). https://doi.org/10.1016/S0301-679X(03)00092-6
23. V. K. Stokes, Phys. Fluids **9**, 1709 (1966). https://doi.org/10.1007/978-3-642-82351-0_4
24. G. Ramanaiah, Wear **54**, 315 (1979). https://doi.org/10.1016/0043-1648(79)90123-6
25. N. B. Naduvinamani and S. T. Fathima, Tribol. Int. **36**, 949 (2003). https://doi.org/10.1016/S0301-679X(03)00092-6
26. P. S. Rao and S. Agarwal, J. Nanofluids **7**, 92 (2018). https://doi.org/10.1166/jon.2018.1420
27. N. B. Naduvinamani, S. Shridevi, and S. Patil, An Int. J. **4**, 313 (2018). https://doi.org/10.1615/SpecialTopicsRevPorousMedia.2018022532
28. N. B. Naduvinmani and B. Kashinath, Lubricat. Sci. **18**, 293 (2006). https://doi.org/10.1002/ls.24
29. Nisha, S. Kesavan, and S. Sangeetha, Int. J. Pure Appl. Math. **111**, 17 (2016). https://doi.org/10.12732/ijpam.v111i1.3
30. G. C. Panchal, H. C. Patel, and H. A. Patel, J. Sci. Res. **13**, 745 (2021) http://dx.doi.org/10.3329/jsr.v13i3.51072